Romanian Reports in Physics, Vol. 57, No. 4, P. 873–887, 2005

POLARIZATION EVOLUTION OF SPATIAL SOLITONS IN PHOTOREFRACTIVE BSO CRYSTALS WITH LARGE OPTICAL ACTIVITY AND ABSORPTION

V. I. VLAD[1], A. PETRIS[1], V. BABIN[2], E. FAZIO[3], M. BERTOLOTTI[3]

[1] *Institute of Atomic Physics, NILPRP-Romanian Center of Excellence in Photonics and The Romanian Academy-CASP, Bucharest, Romania*
[2] *NIOE 2000, Bucharest Romania*
[3] *Universita degli Studi di Roma "La Sapienza", Dept. Energetics and INFM, Roma, Italy*

(Received August 29, 2005)

Abstract. We found out analytical solutions to the propagation equations in photorefractive crystals with nonlinear birefringence, large optical activity and absorption, which show the occurrence of spatial solitons, in the usual orientations with respect to the external electric field. Here, we calculate the Stokes parameters of these solitons and we show their polarization evolutions on the Poincaré sphere, in function of the crystal orientation, propagation distance, the soliton-background-intensity-ratio and the external electric field. The experimental polarization states correspond well to our analytical results and numerical simulations. These results are useful for selection of optimum parameters in spatial soliton generation and for future applications in optical switching, routing and storage.

Key words: spatial solitons, photorefractive materials, optical activity, polarization.

1. ANALYTICAL SOLITON SOLUTIONS IN MODELLING LIGHT PROPAGATION IN PHOTOREFRACTIVE CRYSTALS WITH LARGE OPTICAL ACTIVITY AND ABSORPTION

Light propagation in a non-linear anisotropic material with optical activity and absorption can be described by the wave equation for the electric vector of the optical field, $\vec{E}$, [1–21]:

$$\Delta\vec{E}\left(\vec{r},\ t\right)-\frac{1}{c^2}\cdot\left[\hat{\varepsilon}\otimes\frac{\partial^2\vec{E}}{\partial t^2}+\frac{g}{k}\left(\vec{\nabla}\times\frac{\partial^2\vec{E}}{\partial t^2}\right)\right]-\frac{n_0}{c}\alpha\frac{\partial\vec{E}}{\partial t}=0 \tag{1}$$

where c is the light velocity in vacuum, $\hat{\varepsilon}$ is the symmetric dielectric permittivity tensor of the anisotropic material, $g = 2\rho_0/k$ is the gyration constant, ρ_0 is the optical rotating power, k is the wave vector inside the material, n_0 the refractive index and α is the absorption coefficient.

Considering the classical solution of the form:

$$\vec{E}(\vec{r},t)=\vec{A}_0(\vec{r})\,\mathrm{e}^{-(\alpha/2)z}\cdot\mathrm{e}^{i(kz-\omega t)} \tag{2}$$

and introducing the slowly varying envelope approximation (SVEA), Eq. (1) becomes:

$$2ik\cdot\frac{\partial\vec{A}}{\partial z}+\frac{\partial^2\vec{A}}{\partial x^2}+\frac{\partial^2\vec{A}}{\partial y^2}-k^2\cdot\vec{A}+k^2\hat{\varepsilon}\otimes\vec{A}+ik^2\cdot g\left(\vec{e}_z\times\vec{A}\right)+k^2\cdot\frac{g}{k}\left(\vec{\nabla}\times\vec{A}\right)=0 \tag{3}$$

In a simplified single species model, the photorefractive effect consists of photoionization of some donors and the refractive index modulation by the resulting electric space-charge field (including carrier transport and recombination). In the steady state and drift dominated transport conditions, the change of the dielectric permittivity tensor in function of light intensity is described by a simple equation [2–4, 10, 17]. Crosignani et al [15] found out that, in both (1+1)D and (2+1)D cases, the dependence of the dielectric permittivity tensor on the optical field intensity is given in a good approximation by:

$$\hat{\varepsilon}=[\vec{E}_0\hat{R}\cdot n_0^2]\cdot\left[1+\left(\vec{A}/\sqrt{I_B}\right)^2\right]^{-1}+\hat{\varepsilon}_0,\qquad \hat{\varepsilon}_0=\begin{bmatrix}\varepsilon_{xx} & 0\\ 0 & \varepsilon_{yy}\end{bmatrix} \tag{4}$$

where E_0 is the external electric field applied perpendicularly to the optical beams, along the $0X$ axis, $\hat{R}$ is the electro-optic tensor of the anisotropic material, I_B is the background intensity and ε_0 is the dielectric permittivity tensor in the dark (Fig. 1). We denote:

$$c_1=n_0^2r_{41}E_0=(2/n_0)\Delta n\quad\text{and}\quad c_2=n_0^3r_{41}E_0/\lambda_0=2\Delta n/\lambda_0 \tag{5}$$

with Δn – the refractive index change due to the photorefractive effect (induced birefringence).

The rotation of the light electric vector by the optical activity is more conveniently described by the *wave equation in cylindrical coordinates (scaled to the non-linear birefringence coefficient, c_1):*

$$\begin{aligned}&\xi'=\rho\cos\varphi;\quad \eta'=\rho\sin\varphi;\\ &\zeta'=\zeta=c_1kz;\quad \rho=\sqrt{\xi'^2+\eta'^2}=\sqrt{c_1}k\sqrt{x^2+y^2};\quad \varphi=\arctan(y/x).\end{aligned} \tag{6}$$

At low light intensity levels, the intensity dependent factor from Eq. (4) can be linearly approximated as: $(1 - I/I_B) = 1 - r(I/I_0)$, ($I_0$ – the maximum input intensity, $r = I_0/I_B$). One can find solutions of (3) for two important crystal orientations.

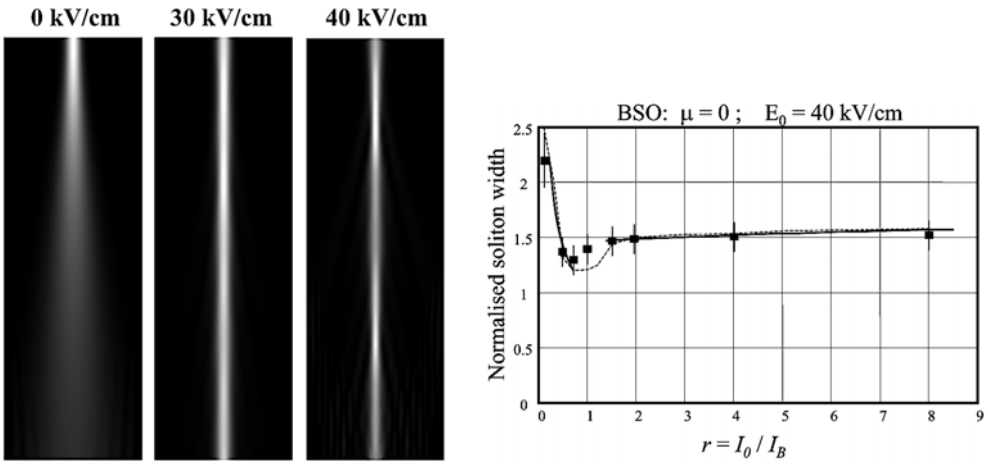

Fig. 1 – (a) The simulation of signal wave propagation in a BSO crystal, for different external electric fields (displayed horizontally) and large propagation distance (six diffraction lengths), which show the soliton formation and the breathing occurrence (at 30 and 40kV/cm). (b) The normalised experimental beam waist versus the signal / background intensity ratio, r, at E_0 = 40 kV/cm, together with the analytical solutions (solid lines) and with numerical solutions of Eq. (14) (dashed line). The normalised waists scales as $(I_0/I_B)^{-1/2}$ for $I_0/I_B < 1$, while scales as $0.06\,(I_0/I_B)^{1/2}$ + bias, for high I_0/I_B (> 2) [26].

Case 1: $\mu = 0$ (electric field oriented along [001] direction). The analytical solution of (3) for the optical field components was found as [10–13]:

$$\begin{bmatrix} A_x \\ A_y \end{bmatrix} = \sqrt{\frac{2I_B r}{\pi}}\, e^{-(\alpha/2)z}\gamma(\varphi,z)\begin{bmatrix} \sin\theta & -\cos\theta \\ \cos\theta & \sin\theta \end{bmatrix}\cdot$$
$$\cdot\begin{bmatrix} \exp\left\{-\left[\rho_1^2 w_0^2/\left(w_0^4+4(8rc_2z)^2\right)\right]\right\}\cdot\left[\pi^2\left(w_0^4+4(8rc_2z)^2\right)\right]^{-1/4} \\ e^{i4rc_2z}\sqrt{2}\,ch^{-1}\left(\cdot\sqrt{2}\rho_1\right)\exp\left\{-\left[{\rho_1}^2/\left(w_0^2+4(8rc_2z)^2/w_0^2\right)\right]\right\}\cdot\left[\pi^2\left(w_0^4+4(8rc_2z)^2\right)\right]^{-1/4} \end{bmatrix} \quad (7)$$

defining a wave, which has a confined core and a weak diffraction part in both components. In (8), w_0 is the normalized input Gaussian beam width,

$$\rho_1 = \sqrt{\frac{2r}{\pi}}\gamma(\varphi,z)\cdot\rho = \sqrt{\frac{2r}{\pi}}\cdot\left|\cos\left(\frac{1}{2}\right)\left(\varphi+gkz-\frac{\pi}{2}\right)\right|^{-1}\cdot\rho = \rho/(\Delta\rho)_1$$

and $(\Delta\rho)_1$ is the normalized beam width (for $r << 1$). The axial factor,

$$\gamma(\varphi,z)\approx\left|\cos\theta\right|^{-1};\quad \theta=(1/2)[\varphi+gkz-(\pi/2)],$$

leads to transverse oscillations ("breathing") of the propagating wave with the period:

$$\lambda_b = 2\lambda / g = 2\pi / \rho_0 .$$

The total intensity of this wave is:

$$\begin{aligned} I(\rho,\varphi,z) &= (2/\pi) I_B(r\gamma^2)\left[\psi_x^2 + \psi_y^2\right] \approx \\ &\approx (2/\pi^2 w_0^2) I_B(r\gamma^2) e^{-\alpha z} \exp\left(-2(\rho_1{}^2 / w_0^2)\right)\left[1 + 2ch^{-2}\left(\sqrt{2}\rho_1\right)\right] \end{aligned} \tag{8}$$

The approximation holds for short crystals (BSO crystals usually used, due to large absorption). One can remark that the jumps of γ-function (when $\cos\theta = 0$) are balanced by the exponential factor, so that the total intensity preserves the soliton-like shape. The initial conditions lead to the relation, $w_0 \approx 6r/\pi^{3/2}$ and to small w_0, which are restrictive conditions for (2+1)D solitons.

One can remark that the soliton-like propagation is maintained in the presence of optical activity and absorption, with better confinement at higher external electric fields. The increase of optical activity (at given absorption coefficient) decreases the soliton breathing period and the increase of absorption coefficient (at a given optical activity) slightly increases the soliton breathing period with a simultaneous increase of soliton width and attenuation.

The soliton width is obtained by combining the maximum width of the hyperbolic secant and the width of the gaussian function of Eq. (8). We can observe that the soliton maximum width is smaller than the gaussian input beam (as expected) and decreases also with the increase of the beam ratio, *r*. Transverse variables are normalized by factor $k\sqrt{n_0^2 r_{41} E_0} = (2\pi n_0^2/\lambda_0)\sqrt{r_{41}E_0}$; thus, one can obtain the soliton maximum width as $w_{s\max} = (\Delta\rho_t)/k\sqrt{n_0^2 r_{41} E_0}$ and deduce its decrease when the external electric field is increased.

Case 2: μ = –1 (electric field oriented along [110] direction). The optical field components (for cubic crystals) are [10–13]:

$$\begin{bmatrix} A_x \\ A_y \end{bmatrix} = \sqrt{\frac{2I_B r}{\pi}}\,\gamma(\varphi, z)\begin{bmatrix} \sin\theta & -\cos\theta \\ \cos\theta & \sin\theta \end{bmatrix}\cdot\begin{bmatrix} e^{-i4rc_2 z}\,\psi_x(\rho_1, z) \\ e^{i4rc_2 z}\,\psi_y(\rho_1, z) \end{bmatrix} \tag{9}$$

with

$$\begin{aligned} \psi_x(\rho_1, z) &= (\psi_{x0}/2) e^{-(\alpha/2)z}\left[(4/3)\left[-ch\rho_1 + \ln\left|th(\rho_1/2)\right|\right]^{-1} - (ch\rho_1)^{-1}\right] \\ \psi_y(\rho_1, z) &= (\psi_{y0}/2) e^{-(\alpha/2)z}\left[(4/3)\left[-ch\rho_1 + \ln\left|th(\rho_1/2)\right|\right]^{-1} + (ch\rho_1)^{-1}\right] \end{aligned} \tag{10}$$

which is **a breathing soliton-like wave** along both axes. Considering the initial conditions (the identity with the 2D symmetrical gaussian input beam):

$\psi_{x0} = \psi_{y0} = \psi_0 = (2\sqrt{\pi}/w_0)^{1/2}$, the soliton-like beam intensity is:

$$I(\rho, \varphi, z) = A_x^2 + A_y^2 =$$

$$= \frac{1}{\sqrt{\pi} w_0} I_B e^{-\alpha z} \cdot r\gamma^2(\varphi, z) \left\{ (16/9) \left[\left| \ln \left| th\left(\frac{\rho_1}{2} \right) \right| - ch\rho_1 \right| \right]^{-2} + (ch\rho_1)^{-2} \right\}. \quad (11)$$

One can remark that, for this crystal orientation, the *y*-component is a transversely modulated (breathing) soliton and the *x*-component is a deformed version of the former one due to the logarithmic term. The same initial conditions lead to a relation between the input beam width and the beam ratio, *r*, namely: $w_0^2 = \pi/2r$, which confirms the restrictive conditions for (2+1)D solitons observed in experiments with other materials.

At high light intensity levels, the intensity dependent factor from Eq. (4) (proportional to the spatial charge field in the photorefractive crystal) can be approximated as:

$$E_{SC} \sim \frac{1}{1 + (I/I_B)} \sim \frac{1}{(I/I_B)} = \frac{I_0}{r \cdot I}; \quad r = \frac{I_0}{I_B} \quad (12)$$

We change the variables in the propagation equations as:

$$\rho_3 = \rho/(\Delta\rho)_3 = \rho/\left(\sqrt{2r/\pi} \cdot \gamma\right) \approx \left[\sqrt{\frac{\pi}{2r}} \cos\left(\frac{1}{2}\phi + \frac{1}{2} gkz - \frac{\pi}{4} \right) \right] \rho$$

$$d\zeta'' = (\pi/2r) c_1 k \left[\gamma(\varphi, z) \right]^{-2} \cdot dz; \quad (13)$$

$$\zeta'' = \left(\frac{\pi^2 n_0^3 r_{41} E_0}{2r\lambda_0} \right) \cdot \left[z + \frac{1}{2\rho_0} \sin(\varphi + \rho_0 z) \cdot \sin(\rho_0 z) \right].$$

Case 1: $\mu = 0$. From Eqs. (3) and (12), one can obtain the solutions [10–13]:

$$\begin{bmatrix} A_x \\ A_y \end{bmatrix} = \sqrt{\frac{2I_B r}{\pi}} \gamma(\varphi, z) \begin{bmatrix} \sin\theta & -\cos\theta \\ \cos\theta & \sin\theta \end{bmatrix} \begin{bmatrix} \psi_x(\rho_3, z) \\ e^{i\zeta''/2} \cdot \psi_y(\rho_3, z) \end{bmatrix} \quad (14')$$

with

$$\psi_x(\rho_3, \varphi, z) = e^{-(\alpha/2)z} \exp\left\{ -\left[\rho_3^2 w_0^2 / \left(w_0^4 + 4\zeta''^2 \right) \right] \right\} \cdot \left[\pi^2 \left(w_0^4 + 4\zeta''^2 \right) \right]^{-1/4}$$

$$\psi_y(\rho_3, \varphi, z) = \pm \frac{\sqrt{2}\,\psi_x}{ch\left[\rho_3 - S_h^2/(1 + S_h^2) \right]}; \quad S_h^2 = \sqrt{\frac{\pi^2}{2w_0^4} \cdot \left(w_0^4 + 4\zeta''^2 \right) \psi_x(0, \varphi, z) - 1}. \quad (14)$$

Assuming that the usual crystal length is small (to have acceptable attenuation) and discarding the beam bending along the propagation axis (given by a small S_h), the total intensity of this soliton-like wave takes the form:

$$I(\rho_3, \varphi, z) = (2/\pi) I_B(r\gamma^2)\left[\psi_x^2 + \psi_y^2\right] \approx$$
$$\approx (2/\pi^2 w_0^2) I_B(r\gamma^2) e^{-\alpha z} \exp\left(-2\rho_3^2 / w_0^2\right)\left[1 + 2ch^{-2}\left(\sqrt{2}\rho_3\right)\right]. \tag{15}$$

The total intensity from Eq. (15) is apparently similar to that obtained at low intensity. However, the dependence of ρ_3 on the axial function γ is different in this situation. One can remark that the soliton-like propagation is maintained here in the presence of optical activity, with better confinement at higher external electric fields. The increase of optical activity decreases the soliton breathing period.

We can remark that, at the propagation distances for which $\gamma \to \infty$, the solution (14) cannot hold and the y-component should be replaced as well by the diffraction solution derived directly from the propagation equations leading to:

$$I(\rho, \varphi, z) \approx 2e^{-\alpha z} \exp\left\{-\left[2\rho^2 w_0^2 / \left(w_0^4 + 4\zeta''^2\right)\right]\right\} \cdot \left[\pi^2\left(w_0^4 + 4\zeta''^2\right)\right]^{-1/2}. \tag{16}$$

Thus, in these points, the wave intensity loses the confinement and tends to the linear diffracting limit.

Case 2: μ = –1. One can derive, as for the low intensity case, the optical field components, solutions of the propagation equations as [10–13]:

$$\begin{bmatrix} A_x(\rho_3, \zeta'') \\ A_y(\rho_3, \zeta'') \end{bmatrix} = \sqrt{\frac{2I_B r}{\pi}} e^{-(\alpha/2)z} \gamma(\varphi, z) e^{-K_1(\rho_3)} \begin{bmatrix} \sin\theta & -\cos\theta \\ \cos\theta & \sin\theta \end{bmatrix} \times$$
$$\times \begin{bmatrix} e^{-i\zeta''/2}\cos K_2(\rho_3) & e^{-i\zeta''/2}\sin K_2(\rho_3) \\ -e^{i\zeta''/2}\sin K_2(\rho_3) & e^{i\zeta''/2}\cos K_2(\rho_3) \end{bmatrix} \begin{bmatrix} \psi_x(0, \zeta'') \\ \psi_y(0, \zeta'') \end{bmatrix} \tag{17}$$

where: $K_1(\rho_3) = \left|\dfrac{1 - ch^2 2\beta + \sin^2 2\alpha_1}{\left(ch2\beta + \cos 2\alpha_1\right)^2}\right|$; $K_2(\rho_3) = \left|\dfrac{2 \cdot \sin 2\alpha_1 \cdot sh2\beta}{\left(ch2\beta + \cos 2\alpha_1\right)^2}\right|$,

$$\alpha_1 = \sqrt{\frac{\pi}{2}} \cdot \frac{\psi_x(0, \zeta'')}{\psi_x^2(0, \zeta'') + \psi_y^2(0, \zeta'')} \cdot \rho_3; \quad \beta = -\sqrt{\frac{\pi}{2}} \cdot \frac{\psi_y(0, \zeta'')}{\psi_x^2(0, \zeta'') + \psi_y^2(0, \zeta'')} \cdot \rho_3 \tag{18}$$

and $\psi_x(0, \zeta'')$, $\psi_y(0, \zeta'')$ are the boundary conditions for the optical field envelopes. Eq. (17) allows to calculate the (2+1)D wave intensity:

$$I(\rho_3, \varphi, \zeta'') = A_x^2 + A_y^2. \tag{19}$$

We can remark that at the propagation distances, for which $\gamma \to \infty$, this solution cannot hold and it should be replaced by the solution of the linear system (diffraction) derived directly from the propagation equations. In these points, the

beam intensity width tends to the linear diffracting limit, *i.e.* the channel width is growing up to $\Delta\rho = w_0\sqrt{1+4\zeta^2/w_0^4}$. This periodic behavior does not disturb too much the solitonic confinement in the most part of the propagation process.

The normalised widths of the wave component envelopes are:

$$\rho_{3x} \equiv 2\alpha_1 = \frac{\rho}{\Delta\rho_{3x}};\ \rho_{3y} \equiv -2\beta = -\frac{\rho}{\Delta\rho_{3y}};\ \Delta\rho_{3x} = \left|\Delta\rho_{3y}\right| = (4/\pi)^{1/4}\gamma\sqrt{rw_0}. \qquad (20)$$

The proportionality of the wave widths to $\sqrt{r}$ corresponds to the experimental findings. The initial conditions introduce additional constraints, r higher than but close to 1 and $w_0^3 = r/\pi^{3/2}$, which are important in the experimental observation of these soliton-like waves.

2. STOKES PARAMETERS OF SPATIAL SOLITONS AND THEIR SPACE-TIME EVOLUTION

Previously, we have derived the photorefractive soliton intensity only, discarding its phase. Now, we shall completely write the spatial soliton fields including the phases:

$$A_x = \left|A_x\right|\cdot e^{i\cdot\phi_x};\quad A_y = \left|A_y\right|\cdot e^{i\cdot\phi_y};\quad \phi = \phi_x - \phi_y \qquad (21)$$

and we shall describe the soliton polarization state by the Stokes parameters:

$$\begin{aligned} S_0' &= \left|A_x\right|^2 + \left|A_y\right|^2 = I_x + I_y = I \\ S_1' &= \left|A_x\right|^2 - \left|A_y\right|^2 = I_x - I_y \\ S_2' &= 2\Re e\left(A_x^*\cdot A_y\right) = 2A_xA_y\cos\phi = 2I_{45} - I \\ S_3' &= 2\Im m\left(A_x^*\cdot A_y\right) = 2A_xA_y\sin\phi;\quad S_1'^2 + S_2'^2 + S_3'^2 = S_0'^2, \end{aligned} \qquad (22)$$

where I_{45} is the light intensity "seen" by a polarizer, which is rotated at 45°. We shall use the previous analytical solutions, at high intensity ratios, which were checked experimentally more easily.

Before starting the calculations, we shall introduce the normalization of Stokes parameters to the soliton intensity, in order to use a representation on the Poincaré sphere with unit radius.

For **low intensity** ratios, $r << 1$, using the solutions from (7) and (10), one can derive the Stokes parameters for the above mentioned crystal orientations. One can get easily:

$$\begin{aligned} S_0 &= 1; \\ S_1 &= -I_1 \cos 2\theta - I_2 \sin 2\theta [\cos(\mu - 1)\Delta n \cdot kz / 2n_0^2]; \\ S_2 &= I_1 \sin 2\theta - I_2 \cos 2\theta [\cos(\mu - 1)\Delta n \cdot kz / 2n_0^2]; \\ S_3 &= -I_2 [\sin(\mu - 1)\Delta n \cdot kz / 2n_0^2], \end{aligned} \tag{23}$$

where

$$I_1(\rho_1, z, \varphi) = \frac{\psi_x^2 - \psi_y^2}{\psi_x^2 + \psi_y^2}, \quad I_2(\rho_1, z, \varphi) = \frac{2\psi_x \psi_y}{\psi_x^2 + \psi_y^2} \text{ and } \theta = \frac{1}{2}\left(\varphi + 2\rho_0 z - \frac{\pi}{2}\right). \tag{24}$$

In the case $\mu = 0$,

$$I_1(\rho_1) = \frac{ch^2\left[\left(r/\sqrt{\pi}w_0\right)^{1/2}\gamma\rho_1\right] - 2}{ch^2\left[\left(r/\sqrt{\pi}w_0\right)^{1/2}\gamma\rho_1\right] + 2}; \quad I_2(\rho_1) = \frac{2\sqrt{2}\cdot ch\left[\left(r/\sqrt{\pi}w_0\right)^{1/2}\gamma\rho_1\right]}{ch^2\left[\left(r/\sqrt{\pi}w_0\right)^{1/2}\gamma\rho_1\right] + 2} \tag{24'}$$

with:

$$\lim_{\rho_1 \to 0} I_1(\rho_1) = -1/3; \quad \lim_{\rho_1 \to 0} I_2(\rho_1) = 2\sqrt{2}/3$$

and

$$\begin{aligned} S_0 &= 1; \\ S_1 &= (1/3)\sin(\varphi + 2\rho_0 z) + (2\sqrt{2}/3)\cos(\varphi + 2\rho_0 z)\cdot\cos(4rn_0^3 r_{41}E_0 z/\lambda_0); \\ S_2 &= (1/3)\cos(\varphi + 2\rho_0 z) - (2\sqrt{2}/3)\sin(\varphi + 2\rho_0 z)\cdot\cos(4rn_0^3 r_{41}E_0 z/\lambda_0); \\ S_3 &= (2\sqrt{2}/3)\sin(4rn_0^3 r_{41}E_0 z/\lambda_0). \end{aligned} \tag{25}$$

The representation of soliton polarization evolution on Poincaré sphere for $\mu = 0$ and $r << 1$ is shown in Fig. 2. We have considered spatial solitons in a BSO crystal with the mentioned orientation, with the length $L = 8$ mm and with the following data [20, 34, 35]: $n_0 = 2{,}615$; $r_{41} = 5 \cdot 10^{-12}$ m/V; $\rho_0 = 673{,}7\ \text{m}^{-1}$; $\lambda_0 = 0{,}5145 \times 10^{-6}$ m. One can remark that the polarization trajectory of the spatial soliton in BSO crystal is better confined around the equator for small r (*e.g.* to $r = 1/100$). In this case, the soliton polarization becomes slightly elliptical in propagation, with the long axis rotated by the optical activity. Thus, we can consider that the soliton polarization remains relatively close to the input (linear) one, *i.e.* it is relatively stable.

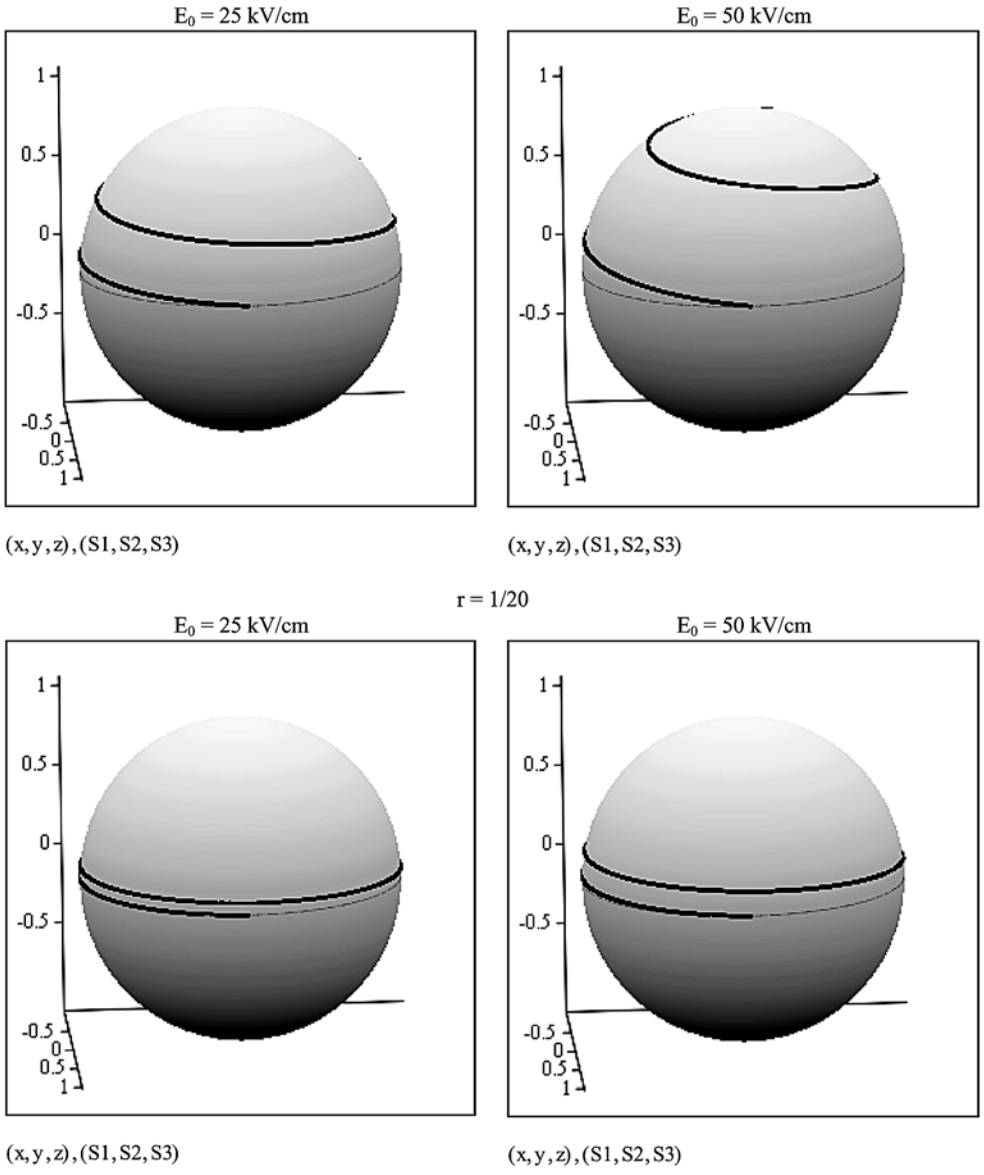

Fig. 2 – Soliton polarization evolution on Poincaré sphere for $\mu = 0$ and $r << 1$.

In the case $\mu = -1$, the Stokes parameters from (23) have the following coefficients:

$$I_1(\rho_1) = \frac{8}{3}\frac{(ch\rho_1)\left[ch\rho_1 - \ln\left|th(\rho_1/2)\right|\right]}{\left[(3/4)ch\rho_1\right]^2 + \left[ch\rho_1 - \ln\left|th(\rho_1/2)\right|\right]^2};$$

$$I_2(\rho_1)=\frac{\left[(4/3)ch\rho_1\right]^2-\left[ch\rho_1-\ln\left|th(\rho_1/2)\right|\right]^2}{\left[(4/3)ch\rho_1\right]^2+\left[ch\rho_1-\ln\left|th(\rho_1/2)\right|\right]^2};\quad \rho_1=\sqrt{2r/\pi}\cdot\gamma\rho. \tag{26}$$

For **high intensity** ratios, $r>>1$, using the solutions from (14) and the definitions from (22), one can derive the Stokes parameters for the above mentioned crystal orientations:

$$\begin{aligned}&S_0=1;\\&S_1=-I_1\cos 2\theta-I_2\sin 2\theta[\cos(\mu-1)\zeta''/2];\\&S_2=I_1\sin 2\theta-I_2\cos 2\theta[\cos(\mu-1)\zeta''/2];\\&S_3=-I_2[\sin(\mu-1)\zeta''/2],\end{aligned} \tag{27}$$

where

$$\zeta''=\left(\frac{\pi^2n_0^3r_{41}}{2r\lambda_0}\right)\cdot\left[z+\frac{1}{2\rho_0}\sin\left(\varphi+\rho_0z\right)\cdot\sin\left(\rho_0z\right)\right]E_0=\omega_E(z)E_0$$

$$I_1(\rho_3,z,\varphi)=\frac{\psi_x^2-\psi_y^2}{\psi_x^2+\psi_y^2},\ I_2(\rho_3,z,\varphi)=\frac{2\psi_x\psi_y}{\psi_x^2+\psi_y^2}\ \text{and}\ \theta=\frac{1}{2}\left(\varphi+2\rho_0z-\frac{\pi}{2}\right).$$

Case μ = 0. First, one can calculate the coefficients:

$$I_1\left(\rho_3\right)\approx\frac{ch^2\rho_3-2}{ch^2\rho_3+2};\quad I_2\left(\rho_3\right)\approx\frac{2\sqrt{2}\cdot ch\rho_3}{ch^2\rho_3+2} \tag{28}$$

and one can remark that:

$$\lim_{\rho_3\to 0}I_1\left(\rho_3\right)\approx-1/3;\quad \lim_{\rho_3\to 0}I_2\left(\rho_3\right)\approx 2\sqrt{2}/3. \tag{29}$$

Close to the optical axis, soliton Stokes parameters are:

$$\begin{aligned}&S_0(z)=1;\\&S_1(z)=(1/3)\sin\left(\varphi+2\rho_0z\right)+\left(2\sqrt{2}/3\right)\cos\left(\varphi+2\rho_0z\right)\cdot\cos\left[E_0\omega_E(z)/2\right];\\&S_2(z)=+(1/3)\cos\left(\varphi+2\rho_0z\right)-\left(2\sqrt{2}/3\right)\sin\left(\varphi+2\rho_0z\right)\cdot\cos\left[E_0\omega_E(z)/2\right];\\&S_3(z)=\left(2\sqrt{2}/3\right)\sin\left[E_0\omega_E(z)/2\right].\end{aligned} \tag{30}$$

For low optical activity, $\rho_0\approx 0$, one can find: $\omega_E(z)\approx\left[\frac{\pi^2n_0^3r_{41}}{2r\lambda_0}\right]\cdot z\left(1+\frac{\sin\varphi}{2}\right)$. Moreover, the small values of the electro-optical coefficient of the BSO crystals lead to $\omega_E<<1$ (at reasonable crystal lengths).

The representation of soliton polarization evolution on Poincaré sphere for $\mu = 0$ and $r >> 1$ is shown in Fig. 3, for a BSO crystal with the same orientation and parameters as considered in in the case $\mu = 0$ and $r << 1$. One can remark that the polarization trajectory of the spatial soliton in BSO crystal is better confined

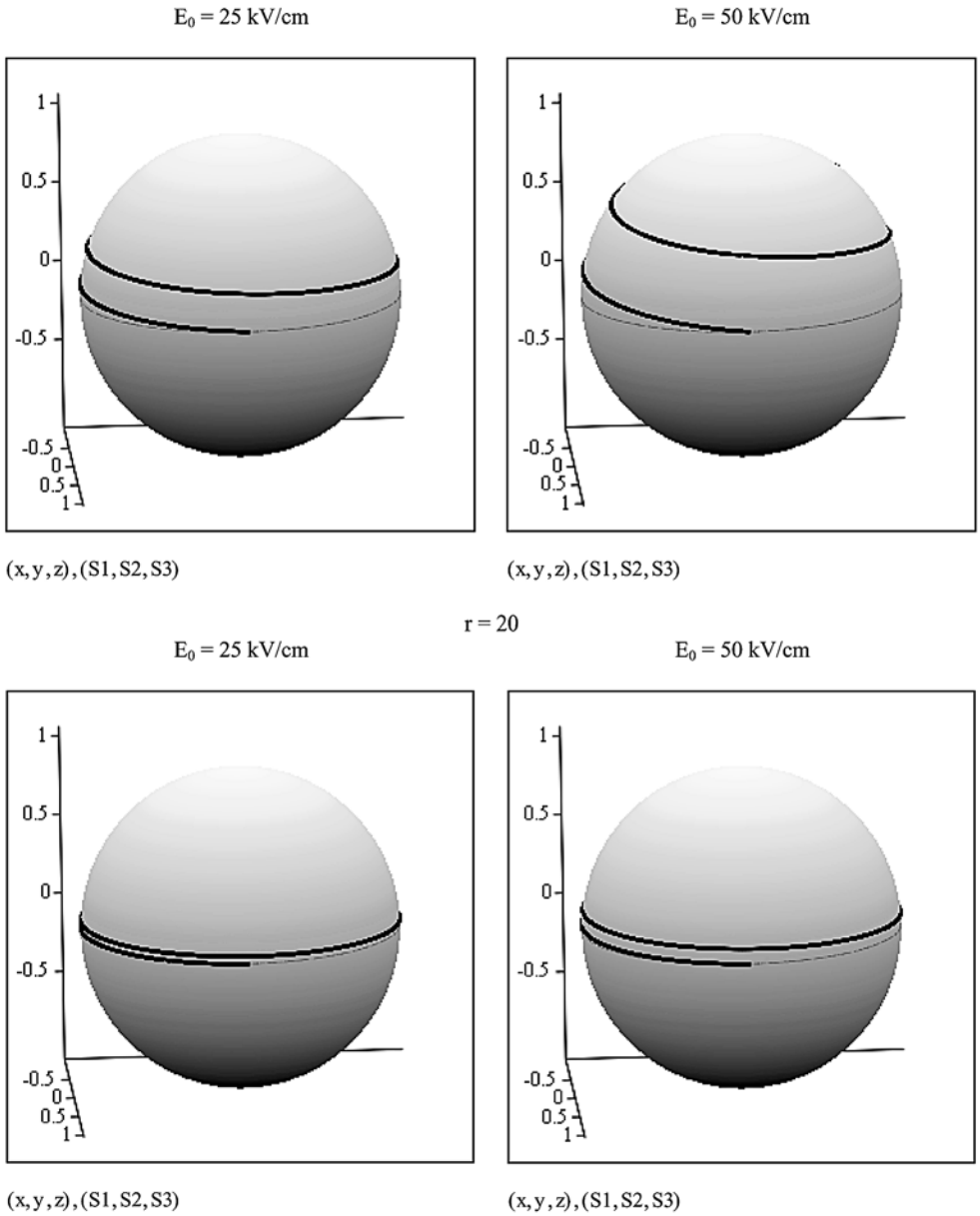

Fig. 3 – Soliton polarization evolution on Poincare sphere for $\mu = 0$ and $r >> 1$.

around the equator for large r (*e.g.* to $r = 100$). In this case, the soliton polarization becomes slightly elliptical in propagation, with the long axis rotated by the optical activity (similarly to the behavior shown for $\mu = 0$ and very small r). Again, we can consider that, for large r, the soliton polarization remains relatively close to the input (linear) one, *i.e.* it is relatively stable.

Case $\mu = -1$. The Stokes parameters take the form:

$$\begin{aligned}
&S_0(z) = 1;\\
&S_1(z) = -I_1(\rho_3)\sin(\varphi + 2\rho_0 z) + I_2(\rho_3)\cos(\varphi + 2\rho_0 z)\cdot\cos\left[E_0\omega_E(z)\right];\\
&S_2(z) = -I_1(\rho_3)\cos(\varphi + 2\rho_0 z) - I_2(\rho_3)\sin(\varphi + 2\rho_0 z)\cdot\cos\left[E_0\omega_E(z)\right];\\
&S_3(z) = I_2(\rho_3)\sin\left[E_0\omega_E(z)\right];
\end{aligned} \tag{32}$$

with the coefficients:

$$\begin{aligned}
&I_1(\rho_3,\zeta'') =\\
&= \frac{2\psi_x(0,\zeta'')\psi_y(0,\zeta'')\cdot\sin(2K_2(\rho_3)) + \left[\psi_x^2(0,\zeta'') - \psi_y^2(0,\zeta'')\right]\cdot\cos(2K_2(\rho_3))}{\left[\psi_x^2(0,\zeta'') + \psi_y^2(0,\zeta'')\right]} =\\
&= \sin(2K_2)\\
&I_2(\rho_3,\zeta'') =\\
&= \frac{2\psi_x(0,\zeta'')\psi_y(0,\zeta'')\cdot\cos(2K_2(\rho_3)) - \left[\psi_x^2(0,\zeta'') - \psi_y^2(0,\zeta'')\right]\cdot\sin(2K_2(\rho_3))}{\left[\psi_x^2(0,\zeta'') + \psi_y^2(0,\zeta'')\right]} =\\
&= \cos(2K_2)
\end{aligned} \tag{33}$$

One can remark that:

$$\lim_{\rho_3\to 0} I_1(\rho_3) = 0; \quad \lim_{\rho_3\to 0} I_2(\rho_3) = 1. \tag{34}$$

and in this case, close to the optical axis, soliton Stokes parameters are:

$$\begin{aligned}
&S_0(z) = 1\\
&S_1(z) = \cos(\varphi_0 + 2\rho_0 z)\cdot\cos(E_0\omega_E(z))\\
&S_2(z) = -\sin(\varphi_0 + 2\rho_0 z)\cdot\cos(E_0\omega_E(z))\\
&S_3(z) = \sin(E_0\omega_E(z)).
\end{aligned} \tag{35}$$

Finally, we have studied the dependence of the soliton Stokes parameters on the external electric field, for BSO crystals with orientation $\mu = 0$. The theoretical curves are calculated with Stokes parameters from eqs. (29) and (30) and with the

variable φ fixed at its value in the output plane, in the absence of external electric field, $\varphi = \varphi_L = arctg\left[\frac{S_{1L} - 2\sqrt{2}\ S_{2L}}{S_{2L} + 2\sqrt{2}\ S_{1L}}\right] - 2\rho_0 L.$

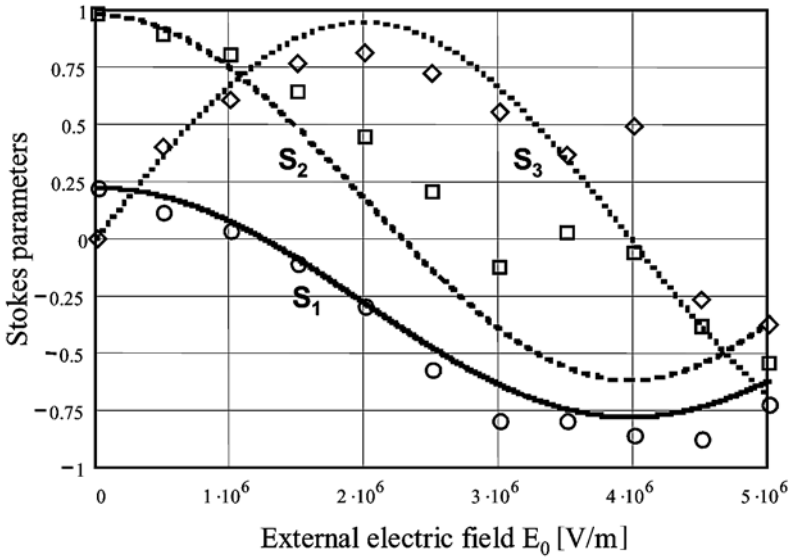

Fig. 4 – The dependence of the soliton Stokes parameters on the external electric field, for a BSO crystal with orientation $\mu = 0$ and L = 8 mm. Here, the experimental data for S_1 is represented by circles, for S_2, by squares and for S_3, by rhomb uses. The best fit, with different lines, corresponds to the intensity ratio of $r = 4.5$.

Taking into account the small accuracy in measuring the parameters S_2 and S_3, we can consider that the experimental data for Stokes parameters from Fig. 4, at different electrical fields, are conveniently fitted by the soliton analytical results.

3. CONCLUSIONS

Analytical solutions of the propagation equations in photorefractive crystals with nonlinear birefringence, large optical activity and absorption show the occurrence of spatial solitons, in the usual orientations with respect to the external electric field. Contrary to the common belief, optical activity seems to help soliton formation and stability. These solutions allow the calculation of Stokes parameters (the soliton polarization states) for crystal orientations corresponding to $\mu = 0$ and $\mu = -1$, different propagation distances, soliton/background intensity ratios and external electric fields. The polarization evolution of photorefractive solitons is

complex and arrives at relatively stable cycles within the usual crystal lengths, at high external electric fields and either small or high soliton/background intensity ratios. The theoretical predictions are in good agreement with our experimental and numerical results.

These results have potential applications for optimum spatial soliton generation in optical communication systems (dynamic waveguiding, switching, routing and storage).

Acknowledgements. This work was supported by the Intergovernmental Agreement between the Romanian Ministry for Education and Research and the Italian Ministry for External Affairs in R&D (project # 36), by a CNCSIS grant, by the Romanian Program for Basic Research "CERES" (project #4-221), by the Romanian Academy CASP and FP6-PHOREMOST-NoE IST-2-511616.

REFERENCES

1. M. Segev, B. Crosignani, A. Yariv and B. Fisher, Phys. Rev. Lett., **68**, 923 (1992).
2. G. C. Duree, J. L. Schultz, G. J. Salamo, M. Segev, A. Yariv, B. Crosignani, P. di Porto, E. J. Sharp, R. R. Neurgaonkar, Phys. Rev. Lett., **71**, 533 (1993).
3. D. N. Christodoulides and M. I. Carvalho, J. Opt. Soc. Am. B, **12**, 1628 (1995); Opt. Lett., **19**, 1714 (1994).
4. B. Crosignani, M. Segev, D. Engin, P. di Porto, A. Yariv and G. J. Salamo, J. Opt. Soc. Am., B **10**, 446 (1993).
5. M. D. Iturbe Castillo, P. A. Marquez Aguilar, J. J. Sanchez Mondragon, S. Stepanov and V. Vysloukh, Appl. Phys. Lett. **64**, 406 (1994).
6. B. Crosignani, P. di Porto, M. Segev, G. J. Salamo and A. Yariv, Riv. del Nuovo Cimento, **21**, 1 (1998).
7. M. P. Petrov, S. I. Stepanov and A. V. Khomenko, Photorefractive Crystals in Coherent Optical Systems, Springer V., Berlin, 1991.
8. S. R. Singh and D. N. Christodoulidis, J. Opt. Soc. Am., **B13**, 719 (1996).
9. W. Krolikowski, N. Akhmediev, D. R. Andersen, B. Luther-Davies, Opt. Commun., **132**, 179 (1996).
10. V. I. Vlad, V. Babin, M. Bertolotti, E. Fazio and M. Zitelli, in Programme of OSA Annual Meeting, Santa Clara, 1998, Paper ThCC7, p. 143, 1999; Proc. Romanian Academy, **A1**(1), 25 (2000) and **A1**(3), (2000).
11. E. Fazio, F. Mariani, A. Funto, M. Zitelli, M. Bertolotti, V. Babin and V. I. Vlad, (1+1)D Screening Solitons in Crystals with Strong Optical Activity, Proc. SPIE, **4430**, 411(2001); J. Optics**: A3**, 466 (2001).
12. V. I. Vlad, V. Babin, M. Bertolotti and E. Fazio, Proc. SPIE, **4430**, 418 (2001).
13. E. Fazio, V. Babin, M. Bertolotti and V. I. Vlad, *Soliton-like propagation in photorefractive crystals with strong optical activity*, Phys. Rev. **E**, **66**, 016605 (2002).
14. E. Fazio, W. Ramadan, A. Belardini, A. Bosco, M. Bertolotti, A. Petris, V. I. Vlad, *(2+1)-dimensional soliton formation in photorefractive BSO Crystals*, Phys. Rev. **E**, **67**, 026611 (2003).
15. M. Bertolotti, V. I. Vlad, E. Fazio, V. Babin, A. Petris, *Propagation of spatial solitons in photorefractive crystals with large optical activity and absorption*, Romanian Journal of Physics, **48** (Suppl. I), 125–142 (2003).
16. E. Fazio, W. Ramadan, M. Bertolotti, A. Petris and V. I. Vlad, J. of Optics A: Pure and Appl. Opt., **5**, S119–S123 (2003).

17. W Ramadan, E. Fazio, I. Fakkar, A. Mascioletti, R. Rinaldi, V. I. Vlad and M. Bertolotti, *Stationary self-confined beams at 633 nm in BSO crystals*, J. of Optics A: Pure and Appl. Opt., **6**, S432–436 (2003).
18. V. I. Vlad, E. Fazio and M. Damzen, Guest Editors, *Photorefractive materials and effects for photonics* (Editorial), J. of Optics A: Pure and Appl. Opt., **6**, S387 (2003).
19. V. I. Vlad, E. Fazio, M. Damzen, A. Petris, *Dynamic waveguides and gratings in photorefractive crystals*, Chapter 3, in *Photoexcited processes and applications*, A. Peled, Ed., Kluwer Academic Publ., Amsterdam & NY, 2003, pp. 57–100.
20. E. Fazio, W. Ramadan, A. Bosco, R. Rinaldi, A. Mascioletti, F. Renzi, V. I. Vlad, A. Petris, V. Babin and M. Bertolotti, *Intensity and polarization dynamics of spatial solitons in photorefractive crystals with large optical activity*, Proc. SPIE "ROMOPTO 2003", (Invited Plenary Lecture), **5581**, 51–55 (2004).
21. V. I. Vlad, A. Petris, V. Babin, E. Fazio and M. Bertolotti, *Polarization evolution of spatial solitons in photorefractive crystals with large optical activity*, Proc. SPIE "ROMOPTO 2003", **5581**, 589–599 (2004).